Shimizu *et al. Earth, Planets and Space* (2016) 68:89
DOI 10.1186/s40623-016-0462-9

Earth, Planets and Space

FULL PAPER Open Access

MHD study of three-dimensional spontaneous fast magnetic reconnection for cross-tail plasma inflows in magnetotail

Tohru Shimizu*, Hiroyuki Torii and Koji Kondoh

Abstract

The 3D instability of spontaneous fast magnetic reconnection process is studied with magnetohydrodynamic simulations, where 2D model of the spontaneous fast magnetic reconnection process is destabilized in three dimensions. In this 3D instability, the spontaneous fast magnetic reconnection process is intermittently and randomly caused in 3D. In this paper, as a typical event study, a single 3D fast magnetic reconnection process often observed in the 3D instability is studied in detail. As a remarkable feature, it is reported that, when the 3D fast magnetic reconnection process starts, plasma inflows along the magnetic neutral line are observed, which are driven by plasma static pressure gradient along the neutral line. The plasma inflow speed reaches about 15 in the upstream field region. The unmagnetized inflow tends to prevent the 3D reconnection process; nevertheless, the 3D reconnection process is intermittently maintained. Such high-speed plasma inflows along the neutral line may be observed as dawn–dusk flows in space satellite observations of magnetotail's bursty bulk flows.

Keywords: Magnetic reconnection, Bursty bulk flow, 3D MHD instability, MHD simulation

Introduction

Fast magnetic reconnection process provides a physical mechanism by which magnetic energy is explosively converted into plasma kinetic and thermal energies, resulting in the generation of plasma jets. This mechanism has been considered to play a crucial role in solar flares and geomagnetic substorms. The study of fast magnetic reconnection process includes a lot of tough problems to be resolved because it is related to various complexities hidden in plasma physics for wide scales in time and space. In MHD scale studies, there are two famous models of the magnetic reconnection process (Vasyliunas 1975) which are widely known as the Sweet–Parker-type and Petschek-type models.

In the Sweet–Parker-type reconnection process (Parker 1957), when magnetic field lines are reconnected in a place of the current sheet, the Joule heating generated there increases the plasma pressure, leading to non-uniformity of the plasma pressure in the current sheet. Then, the resulting plasma pressure gradient can accelerate plasma in the current sheet. The place where the Joule heating is effective is called as the magnetic diffusion region. In the Sweet–Parker-type reconnection process, the magnetic diffusion region may be considered to be the whole of plasma jet region.

The Petschek-type reconnection process (Petschek 1964) includes a pair of slow shocks extending from the magnetic diffusion region, which can accelerate plasma. In this type, the magnetic diffusion region must be strongly localized at a place of the current sheet and separated from the plasma jet region where plasma is accelerated by a pair of slow shocks. It is well known (Vasyliunas 1975; Forbes and Priest 1987) that the Petschek-type reconnection process becomes more active than the Sweet–Parker type. To explain solar flares and geomagnetic substorms, the Petschek type is considered to be more suitable than the Sweet–Parker type. However, even in the steady state model, it is impossible to strictly find the analytical solution in the resistive MHD frame, because of the extreme difficulty. Instead, there are many

*Correspondence: shimizu@cosmos.ehime-u.ac.jp
Research Center for Space and Cosmic Evolution, Ehime University, Bunkyo-cho 2-5, Matsuyama, Japan

numerical MHD studies to explore the Petschek-type reconnection process.

Ugai numerically found that the 2D Petschek-type reconnection process can be reproduced with a locally enhanced resistivity which is assumed to be non-uniform in space and constant in time (Ugai and Tsuda 1977). Then, assuming a kind of the current-driven anomalous resistivity instead of the locally enhanced resistivity, Ugai numerically revealed that the 2D Petschek-type fast magnetic reconnection process can be spontaneously established, where a pair of slow shocks, high-speed plasma jets and large-scale magnetic loops, i.e., plasmoids, have been observed (Ugai 1984, 1987a, b). The most important finding was that the destabilized 1D current sheet can be spontaneously developed to the 2D Petschek-type fast magnetic reconnection, due to a kind of the 2D nonlinear tearing instability based on the current-driven anomalous resistivity.

As the computer performance increases, Ugai's 2D model studies have been developed to 3D study (Ugai et al. 2004, 2005; Ugai 2010). However, those Ugai's 3D studies were not a direct extension of his previous 2D studies. For instance, those 3D studies could not address whether the Petschek-type 2D fast magnetic reconnection is unstable or not. Rather, since the initial resistive disturbance employed in his 3D studies was assumed to be strongly localized in the sheet current direction, the resulting fast reconnection process was consequently localized in the sheet current direction. As easily expected, the resulting fast reconnection process becomes full 3D. Hence, in Ugai's 2D and 3D studies, whether the fast reconnection process results in 2D or 3D directly depends on whether the initial resistive disturbance is set as 2D or 3D.

Rather, it is worth examining whether the 2D fast reconnection process studied by Ugai is unstable in 3D. To do so, we examined whether the 2D fast reconnection process can be numerically destabilized in 3D or not. According to our recent papers (Shimizu et al. 2009a, b), it was numerically revealed that the 2D fast reconnection process is essentially unstable in 3D, resulting in the random and intermittent 3D fast reconnection process. In contrast to Ugai's 3D study, our 3D study is a direct extension of the previous his 2D studies (Ugai 1984, 1987a, b; Shimizu and Ugai 2000, 2003).

In our 3D studies, the resulting 3D fast magnetic reconnection process is impulsive and randomly repeated without any externally driven force. Once 2D fast reconnection process is established, the 2D process is spontaneously changed to 3D process via weak 3D resistive disturbances (perturbations). It is a 3D instability of the 2D fast reconnection process. It means that, even in a 1D current sheet, 3D magnetic loops (plasmoids) can be spontaneously and intermittently ejected from the reconnection regions without any distinct 3D externally driven force. This feature may be applicable for the observations of the solar flares and geomagnetotail.

In fact, our study of the 3D fast reconnection process has been applied to the intermittent plasma down flows observed in solar flares (Shimizu et al. 2009c). Then, our latest study (Shimizu and Kondoh 2013) revealed that the 3D fast reconnection process may have to be the Petschek type and also that the 2D Sweet–Parker type is stable in 3D.

In our previous studies (Shimizu et al. 2009a, b, c; Shimizu and Kondoh 2013), we studied some features of the random and intermittent 3D fast reconnection process, but it is still unclear why and how the 3D fast reconnection process is impulsively repeated. In this paper, we extract a typical single event of the random and intermittent 3D fast reconnection process observed in the 3D instability and then focus on the driving mechanism of the single event. The most important finding is that, when a single event of the 3D fast reconnection process starts, the uniformity of the plasma static pressure along the neutral line is destroyed and the reconnection region is strongly localized in the sheet current direction. Then, such non-uniformity of the pressure drives the unmagnetized plasma inflow along the neutral line toward the active reconnection site, i.e., x-point.

In next chapter, the 3D MHD simulation procedures are shown. Then, the overview of the 3D MHD simulation results is briefly shown, which has been published (Shimizu and Kondoh 2013). In this simulation, 3D impulsive fast reconnection process intermittently and randomly appears. Then, focusing on a typical single event observed in the 3D instability, the plasma inflow mechanism along the neutral line is studied in detail. In "Summary and discussions" section, it is discussed that such a plasma inflow may be detected in the space satellite observations of magnetotail.

3D MHD simulations

Procedures of simulation

In this spontaneous fast reconnection model, the reconnection process is initiated by a small resistive disturbance induced in an exactly 1D current sheet. The initial small resistive disturbance is almost 2D on the plane perpendicular to the sheet current direction but includes weak fluctuations (perturbations) in the sheet current direction. Using this initial small resistive disturbance, we can examine whether the 2D fast magnetic reconnection process is stable or not. After the small resistive disturbance is removed in the initial phase of the simulation (at $T = 4$), the thinning of the current sheet spontaneously starts around the most intensive region of the

small resistive disturbance, leading to the enhancement of the current-driven anomalous resistivity assumed after $T = 4$. Then, the fast magnetic reconnection process is spontaneously developed by a nonlinear tearing instability based on the current-driven anomalous resistivity. It is remarkable that, after $T = 4$, any external driven mechanism to push the current sheet is not required to keep the reconnection process. Eventually, the fast reconnection process started as 2D spontaneously changes to fully 3D, because of the 3D instability.

The 3D compressible magnetohydrodynamic (MHD) equations are

$$\begin{aligned} \mathrm{D}\rho/\mathrm{D}t &= -\rho\nabla\cdot\mathbf{u}, \quad \rho\mathrm{D}\mathbf{u}/\mathrm{D}t = -\nabla P + \mathbf{J}\times\mathbf{B}, \\ \partial\mathbf{B}/\partial t - \nabla\times(\mathbf{u}\times\mathbf{B}) &= -\nabla\times(\eta\mathbf{J}), \\ \rho\mathrm{D}e/\mathrm{D}t &= -P\nabla\cdot\mathbf{u} + \eta\mathbf{J}^2, \\ \mathbf{J} &= \nabla\times\mathbf{B}/\mu_0, \quad \nabla\cdot\mathbf{B} = 0, \end{aligned} \tag{1}$$

where $\mathrm{D}/\mathrm{D}t \equiv \partial/\partial t + \mathbf{u}\cdot\nabla$; the gas law, $P = (\gamma - 1)\rho e$, is assumed. e is the internal energy per unit mass, and γ is the specific heat ratio with $\gamma = 5/3$ assumed here. As the Ohm's law, $\mathbf{E} + \mathbf{u}\times\mathbf{B} = \eta\mathbf{J}$ (η is a resistivity) is assumed. The basic equations (1) are transformed to a conservation-law form, and two-step Lax–Wendroff scheme is used for the numerical computation.

The initial current sheet system has exactly 1D structure, i.e., the magnetic field $\mathbf{B} = [B_x(y), 0, 0]$ is assumed as: $B_x(y) = B_{x0}\sin(\pi y/2d_0)$ for $0 < y < d_0$; $B_x = B_{x0}$ for $d_0 < y < Y_1$; $B_x = B_{x0}\cos[(y - Y_1)\pi/1.2]$ for $Y_1 < y < Y_1 + 0.6$); $B_x = 0$ for $y > Y_1 + 0.6$; also, $B_x(y) = -B_x(-y)$ for $y < 0$. Here, $B_{x0} = 1.0$, $d_0 = 1.0$, and $Y_1 = 5.0$, where d_0 is the half width of initial current sheet. The normalization of quantities is self-evident: Distances are normalized by d_0, $\mathbf{B}$ by B_{x0}, and P by $B_{x0}^2/(2\mu_0)$; also, ρ is normalized by the initial uniform plasma density ρ_0, $\mathbf{u}$ by $V_{Ax0}(= B_{x0}/\sqrt{\mu_0\rho_0})$, time t by d_0/V_{Ax0}, current density $\mathbf{J}$ by $B_{x0}/(\mu_0 d_0)$ and so forth. The plasma static pressure $P(y)$ initially satisfies the pressure balance condition,

$$P + B_x^2 = 1 + \beta_0, \tag{2}$$

where β_0 is the ratio of the plasma pressure to the magnetic pressure in the magnetic field region $d_0 < y < Y_1$, where $\beta_0 = 0.15$ is taken. Fluid velocity $\mathbf{u} = (0, 0, 0)$ and plasma density $\rho = 1$ are initially assumed.

For the boundary conditions of the computational region, the symmetry boundary condition is assumed on the yz-plane at $x = 0$, xz-plane at $y = 0$ and xy-planes at $z = 0$ and L_z, so that the computational region is restricted to the first quadrant only and taken to be a square box, $0 \le x \le L_x$, $0 \le y \le L_y$ and $0 \le z \le L_z$. The other boundaries are assumed to be the open (free) boundary where all the quantities are determined by the states of the inner region, so that the first derivatives of the quantities in the direction normal to the boundaries vanish, excepting the normal component of $\mathbf{B}$, which is determined by the solenoidal condition ($\nabla\cdot\mathbf{B} = 0$).

For the numerical conditions in this paper, the computational region $(L_x, L_y, L_z) = (66.0, 13.95, 20.0)$ is taken with the mesh points $(N_x, N_y, N_z) = (750, 640, 100)$, where the numerical mesh size ($\mathrm{D}X$, $\mathrm{D}Y$) is changed in space to concentrate the numerical resolution into the magnetic diffusion region, rather than all other regions, as follows. Firstly, $\mathrm{D}X = 0.04$ is set in $0 < x < 12$ and is set to $\mathrm{D}X = 0.16$ in $42 < x < 66$. In the intermediate region, i.e., $12 < x < 42$, $\mathrm{D}X$ linearly increases from 0.04 to 0.16. Similarly, $\mathrm{D}Y = 0.015$ is set in $0.0 < y < 4.5$ and $\mathrm{D}Y = 0.030$ is set in $6.75 < y < 13.95$. In $4.5 < y < 6.75$, $\mathrm{D}Y$ linearly increases from 0.015 to 0.03. These $\mathrm{D}X$ and $\mathrm{D}Y$ are constant in time, while $DZ = 0.2$ is constant in time and space.

The MHD simulation procedures are basically the same as that of Ugai et al. (2004, 2005), excepting the 3D setup of the initial resistive disturbance. The disturbance is set as follows, to initiate a tearing instability in the current sheet during $0 < T < 4$.

$$\eta_a = 0.04\exp(-\alpha_1(x^2 + y^2))(1 + \alpha_2\cos(\pi z/L_z)) \tag{3}$$

where $\alpha_1 = 0.01$. This disturbance works as a trigger to start the fast magnetic reconnection process. For this resistive disturbance, the magnetic Reynolds number is estimated to be 25 at the origin. When $\alpha_2 = 0.0$ is set, the resulting fast reconnection is exactly 2D. In this paper, we examine the case of $\alpha_2 = 0.01$ where the resistive disturbance is slightly fluctuated only by 1 % in z-direction which is the sheet current direction. This z-directional weak fluctuation works as a perturbation to three-dimensionally destabilize the 2D fast magnetic reconnection process. According to our previous studies, the 2D fast magnetic reconnection process is unstable in three dimensions, as shown below.

The initial resistive disturbance employed by Ugai et al. (2004, 2005) is basically different from one employed here because α_2 in Ugai's 3D studies was much larger. Accordingly, in Ugai's 3D studies, the resulting fast magnetic reconnection directly became 3D, while the resulting fast magnetic reconnection shown in this paper is expected to be approximately 2D. In fact, it is almost 2D on the initial stage, as shown later in Fig. 1a. However, the 2D stage is then developed to 3D stage, as shown in Fig. 1b, c.

After $T = 4$, η_a is removed and, instead, the current-driven anomalous resistivity η_b shown below is set, which spontaneously drives the fast magnetic reconnection process.

$$\eta_b = 0.002(V_\mathrm{d} - V_\mathrm{c}) \quad \text{for } V_\mathrm{d} > V_\mathrm{c} \tag{4}$$

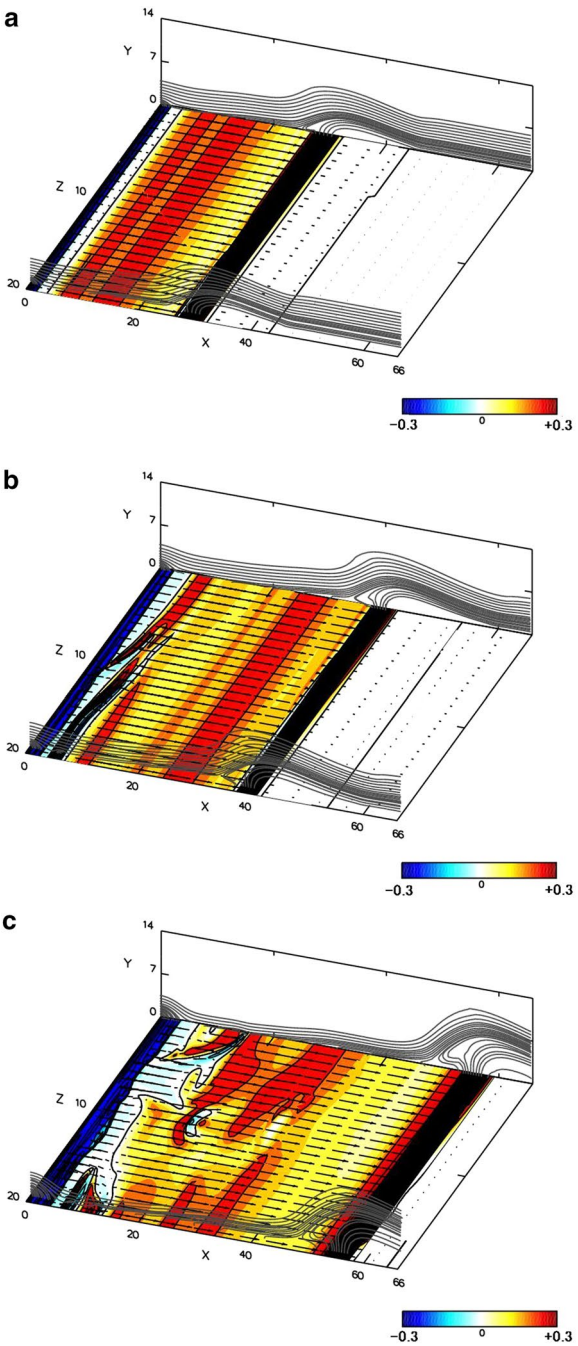

Fig. 1 B_y contour maps on xz-plane at $y = 0$, and magnetic field lines traced at $z = 0$ and $20(=L_z)$. Each figure is for $T = 72$ (**a**), 90 (**b**), and 120 (**c**)

$$\eta_b = 0 \quad \text{for } V_d < V_c \tag{5}$$

where $V_d = |J|m/e\rho$ is the absolute value of the ion–electron drift velocity, i.e., $V_d = |V_i - V_e|$ and $V_c = 4.0$ is set, where V_i and V_e are, respectively, the proton and electron averaged velocity. As additional definitions, $m = m_i + m_e$ is the total mass of proton and electron, where m_i is the proton mass and m_e is the electron mass, in which e is the elementary charge. Note that V_d is not considered in the MHD equation (1) but may be related to the plasma mass density $\rho = \rho_i + \rho_e$ with $\rho_i = n_i m_i$ and $\rho_e = n_e m_e$, where n_i and n_e are, respectively, the proton and electron number density. The current density J is obtained from $\nabla \times \mathbf{B}/\mu_0$, which is 1.57 at the center of the initial current sheet, i.e., $y = 0$. When Eqs. (4) and (5) effectively work, the resulting magnetic Reynolds number reaches about 70 at the most active magnetic neutral point.

Overview of simulation

This simulation starts from an exactly 1D antiparallel magnetic field configuration. At $T = 0$, an initial resistive disturbance is put by Eq. (3) and is kept until $T = 4$. At $T = 4$, the initial resistive disturbance is removed, and instead, Eqs. (4) and (5) are put as the current-driven type anomalous resistivity. Since Eq. (3) is almost 2D, the resulting fast reconnection is expected to be 2D. In fact, the 2D fast reconnection process is observed until about $T = 70$. However, beyond $T = 72$, 3D fast reconnection process abruptly starts.

Figure 1 shows some magnetic field lines and B_y contour map on xz-plane at $y = 0$, i.e., the initial neutral sheet. Red color regions of the contour map mean positive B_y intensity, and blue color regions mean negative B_y intensity. Since $B_y = 0$ is initially set on the xz-plane, the whole of the contour map at $T = 0$ (not shown here) is colored by white. Accordingly, the nonzero B_y intensity observed as red or blue colored regions is generated by the reconnection process.

Figure 1a shows that 2D fast reconnection process generates a 2D plasmoid at $T = 72$, where the B_y contour map is almost uniform in z-direction, i.e., the sheet current direction. Note that the z-directional black wide bands around $x = 0$ and $x = 30$ may be a little confusing, where a lot of contour lines are highly condensed. Indeed, the black wide band around $x = 0$ is colored by blue and the black wide band around $x = 30$ is colored by red. Also, the magnetic field lines are almost the same between at $z = 0$ and L_z. Hence, the fast reconnection process is 2D at this time.

Then, 3D instability of the 2D fast reconnection process abruptly starts beyond $T = 72$, triggered by the z-directional weak fluctuation included in Eq. (3). Figure 1b shows that the B_y contour map becomes non-uniform in z-direction around $0 < x < 10$ at $T = 90$, due to the 3D instability. Finally, Fig. 1c shows the fully destabilized 3D fast reconnection process at $T = 120$.

Some red color regions observed in the B_y contour map mean the formations of 2D and 3D plasmoids. The 2D plasmoid observed as a z-directionally uniform structure

in $30 < x < 40$ of Fig. 1a at $T = 72$ has reached around $50 < x$ in Fig. 1c at $T = 120$. Roughly estimating, the propagation speed of the 2D plasmoid is about 50 % of the Alfven speed measured in the upstream field region, which is slower than the Alfven speed because of the compressibility. Also, some of 3D plasmoids observed as z-directionally non-uniform structures tend to propagate to the positive x-direction, but the dynamics is complex because of the interactions between those plasmoids. The further detail of this simulation result has been reported in our previous work (Shimizu et al. 2009c; Shimizu and Kondoh 2013).

Figure 2a–c, respectively, shows the contour maps of B_y, ηJ and U_z on xz-plane at $y = 0$ at $T = 90$, where the roughly half size ($0 < x < 30.9 \simeq L_x/2$) of the simulation box is only shown. The B_y contour map shown in Fig. 2a is the same as the contour map of the half region of Fig. 1b, excepting the slightly different color scale. Figure 2b shows the contour map of ηJ which is the resistive electric field, i.e., the reconnection rate, where the blue regions have the negative intensity of ηJ. Those negative high-intensity regions are the active reconnection regions indicated by arrows named as event-1, 2 and 3. The solid lines drawn in Fig. 2a–c are the neutral lines so that they separate the red and blue regions in Fig. 2a. These neutral lines are either the x-line or o-line. The o-line is the center of the plasmoid. The neutral lines indicated by arrows of event-1, 2 and 3 are the x-line.

Figure 2c shows the contour map of the sheet current directional plasma flow U_z, where the blue regions have negative value and the red regions have positive value. In other words, the plasma flows in the blue regions are directed downward on this panel and the flows in the red regions are upward. Since U_z is initially zero, the appearance of these red and blue regions in Fig. 2c means a result of the 3D instability. These z-directional plasma flow patterns of event-1 and 2 mean "inflow" toward the active 3D reconnection site because these flows are directed to each high-ηJ -intensity region pointed by the arrows of event-1 and 2. If the flow pattern were "outflow," the location of red and blue regions must be reversed along the x-line, while the z-directional flow pattern in event-3 seems to be directed upward all over the x-line which is covered by red region in Fig. 2c. Hence, the z-directional flow pattern in event-3 is not necessarily recognized to be "inflow." The detection of the inflow pattern is summarized in Table 1.

The format of Fig. 3 is the same as that of Fig. 2, excepting at $T = 108$. Figure 3a shows the location of the

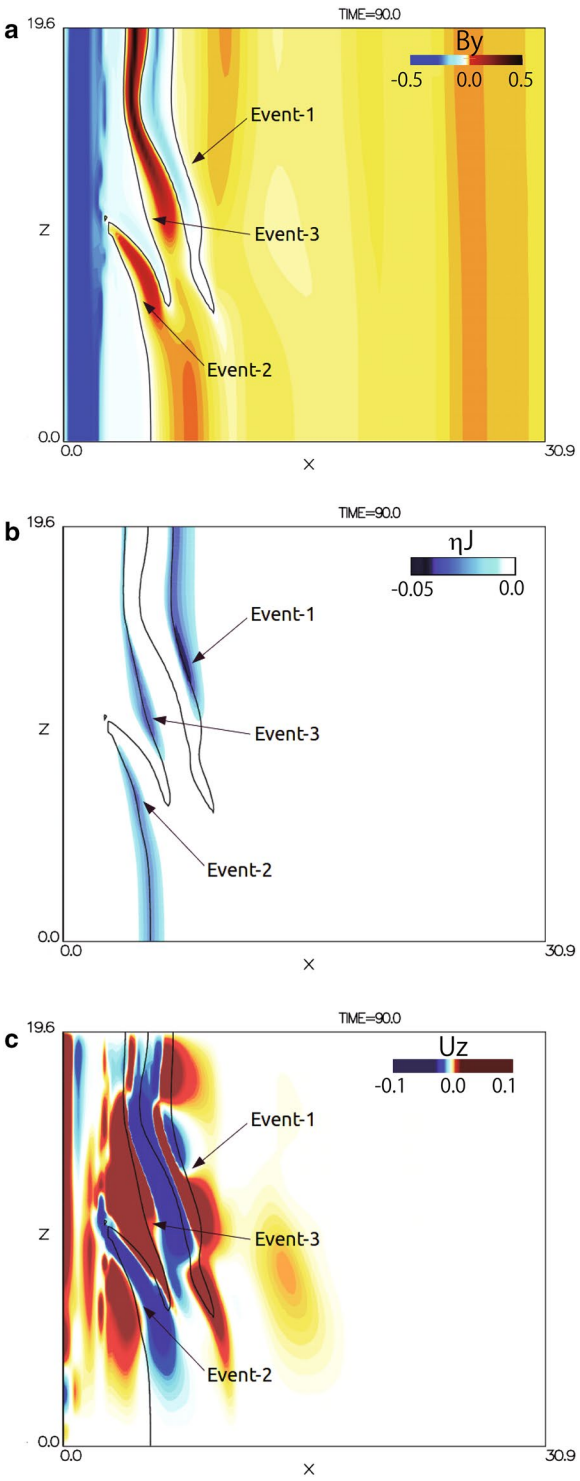

Fig. 2 The contour maps of B_y (**a**), ηJ (**b**), U_z (**c**) for the first, second, and third 3D events at $T = 90$

Table 1 List of 3D events detected in this simulation run

3D event no.	ηJ-peak	Time	x	z	Inflow ?
1	−0.0510	90.0	7.64	13.28	○
2	−0.0444	90.0	4.72	6.70	○
3	−0.0470	91.5	5.71	9.98	×
4	−0.0433	108.0	9.85	6.10	○
5	−0.0400	115.5	15.53	9.42	○
6	−0.0427	117.0	6.43	19.52	○
7	−0.0605	118.5	9.18	19.52	○
8	−0.0580	120.0	15.66	0.57	○
9	−0.0524	121.5	13.70	19.51	○
10	−0.0401	124.5	13.31	16.91	×
11	−0.0473	124.5	11.28	5.25	○
12	−0.0413	124.5	7.43	0.00	×
13	−0.0542	126.0	15.90	5.76	○
14	−0.0536	127.5	11.65	0.00	○
15	−0.0400	129.0	7.94	10.55	○

neutral line as the solid line separating red ($B_y > 0$) and blue ($B_y < 0$) regions. Those neutral lines are also drawn in Fig. 3b. In Fig. 3b, some high-ηJ -intensity regions can be observed. One of those high-intensity regions are marked as event-4. Some other high-intensity regions observed in Fig. 3b have relatively weak (lighter blue) intensity ($0 > \eta J > -0.035$), and the remainders are the remnants of event-1, 2 and 3. In Fig. 3c, we can recognize that the z-directional plasma flows marked as event-4 are "inflow pattern" toward the active reconnection site, like event-1 and 2.

Figure 4 also shows contour maps similar to those of Figs. 2 and 3 but at $T = 115.5$, where another active reconnection site is marked as event-5. As shown in Fig. 4c, event-5 also has the inflow pattern along the x-line like event-1, 2 and 4. At this time, many active events are observed, but the others of event-5 observed in this figure are either the remnants of event-1, 2, 3 and 4 or the beginning phase of event-6, 7 and so on, which are listed in Table 1. The z-scale sizes of event-1, 2 and 3 are observed to be relatively larger than those of the subsequent events. It suggests that this 3D instability includes a kind of the cascade process. In other words, the z-scale size of these events is not directly dominated by the z-scale size L_z in the initial resistive disturbance Eq. (3). What determines the z-scale size is our future work to be resolved.

In this simulation run, every active 3D event detected with a criterion of $\eta J < -0.035$ is summarized in Table 1, including event-1, 2, 3, 4 and 5. This table shows the detection time and location for each event when the maximum value of $|\eta J|$ was observed. As shown in Table 1, the total number of detected events finally reached 15.

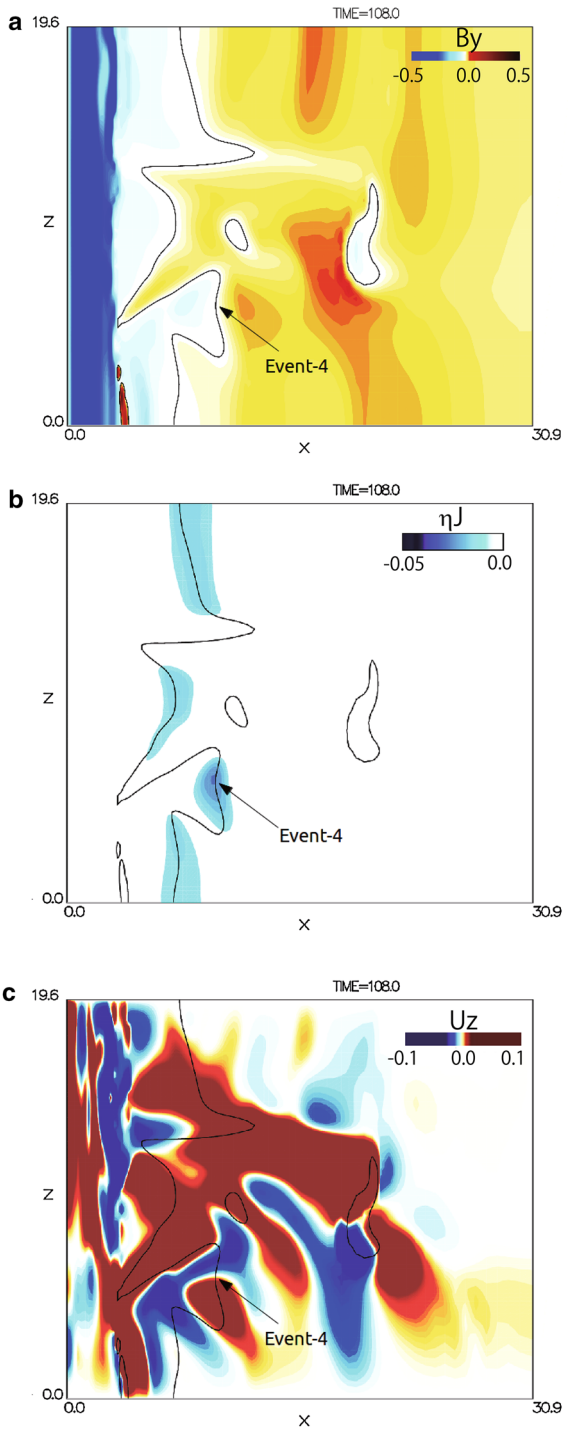

Fig. 3 The contour maps of B_y (**a**), ηJ (**b**), and U_z (**c**) for the fourth 3D event at $T = 108$

As shown in Figs. 2c, 3c and 4c, the z-directional flow patterns along the neutral line in event-1, 2, 4 and 5 are observed to be inflow. In "Inflow" column of Table 1, a circle symbol is put when such z-directional inflow

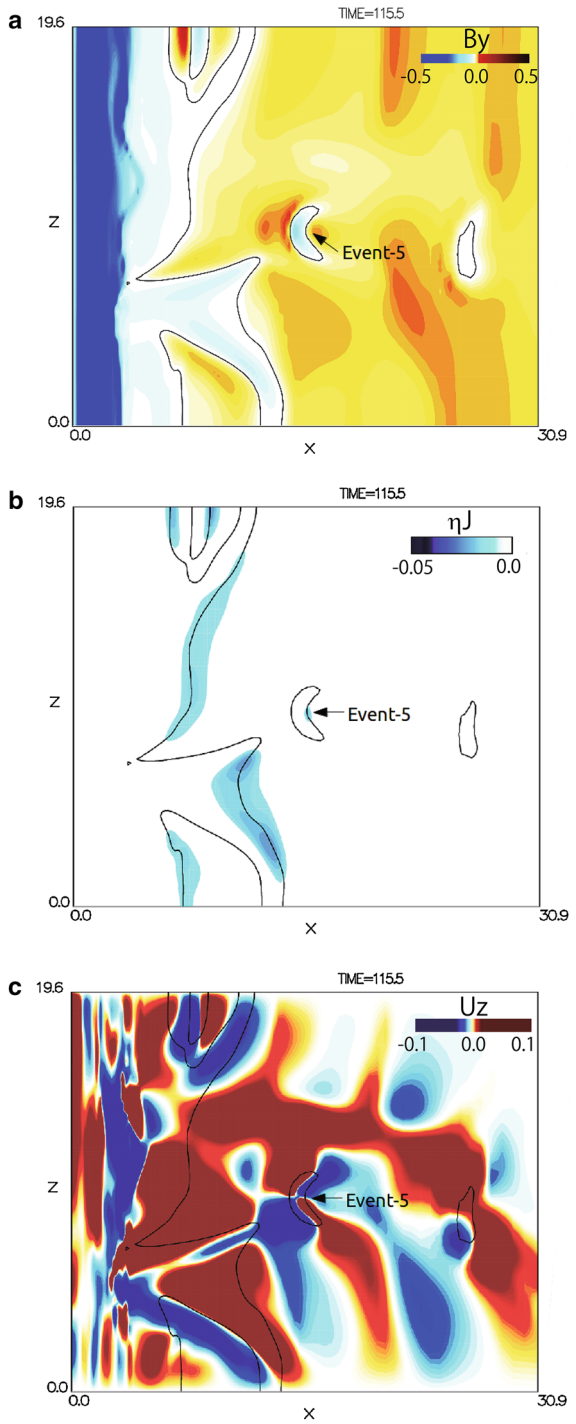

Fig. 4 The contour maps of B_y (**a**), ηJ (**b**), and U_z (**c**) for the fifth 3D event at $T = 115.5$

was detected. Among these 15 events, such inflow pattern was observed in 12 events. Hence, we can say that the inflow pattern is often detected. In the next section, event-5 is studied in detail.

A typical event study of the 3D fast reconnection

In this section, we focus on event-5 listed in Table 1. In comparison with the other events, the location of event-5 is clearly isolated from the other events, so that event-5 is caused as a single event, as shown in Fig. 4a, b. Hence, event-5 will be suitable to study the basic features of this complex 3D instability. At this point, since this 3D instability is random and complex, the basic features may be easily masked by interactions between those events caused nearby.

Figure 5 shows the contour maps of B_y, ηJ and U_z enlarged for event-5 at $T = 120$, which are also shown in Fig. 4. The arrows in Fig. 5a–c are the plasma flow field (U_x, U_z) on the xz-plane of $y = 0$, i.e., the neutral sheet plane. Figure 5a shows the contour map of the reconnected field intensity B_y with red ($B_y > 0$) and blue ($B_y < 0$) colors, like Fig. 4a. A closed-loop solid line A–B–C–D–E–A in Fig. 5a is the neutral line separating the red and blue regions. The same neutral line is also drawn in Fig. 5b, c. As shown in ηJ contour map of Fig. 5b, point D is the most active neutral point because ηJ takes a negative peak which is colored by the deepest blue at the place. Figure 5c shows the U_z contour map, which is also similarly observed in the corresponding region of Fig. 4c. Around point D, the inflow pattern is observed along the neutral line, as discussed in Fig. 4c. As shown in Fig. 5, event-5 is roughly symmetry for the horizontal solid line connecting points B and D. If event-5 interacted with the other events, such symmetry would be destroyed. Hence, it is recognized that event-5 is a single event and almost does not interact with the other events. The details for event-5 have been also studied in Figures 10, 11, 12 and 13 of our previous paper (Shimizu and Kondoh 2013).

Figure 6 schematically shows the topology of some magnetic field lines for event-5 on the B_y intensity contour map of xz-plane at $y = 0$ at $T = 120$. Those traced field lines are started on the symmetry line B–D in Fig. 5a. The B_y contour map is the same as that of Fig. 5a, excepting the slightly different color scale. Considering the symmetry boundary condition at xz-plane of $y = 0$, point B is the o-point and point D is the x-point. Hence, line A–B–C in Fig. 5a is the o-line and line A–E–D–C is the x-line. Note that o-line is the center of the plasmoid. In this simulation run, since B_z component is initially zero and relatively weak even after the onset of the 3D instability, every active x-line is almost parallel to z-axis, where is the active magnetic diffusion region with nonzero ηJ. For example, the blue shaded solid lines in Figs. 2b, 3b and 4b are the active x-lines and all other uncolored solid lines are either the inactive x-line or o-line, where ηJ is zero.

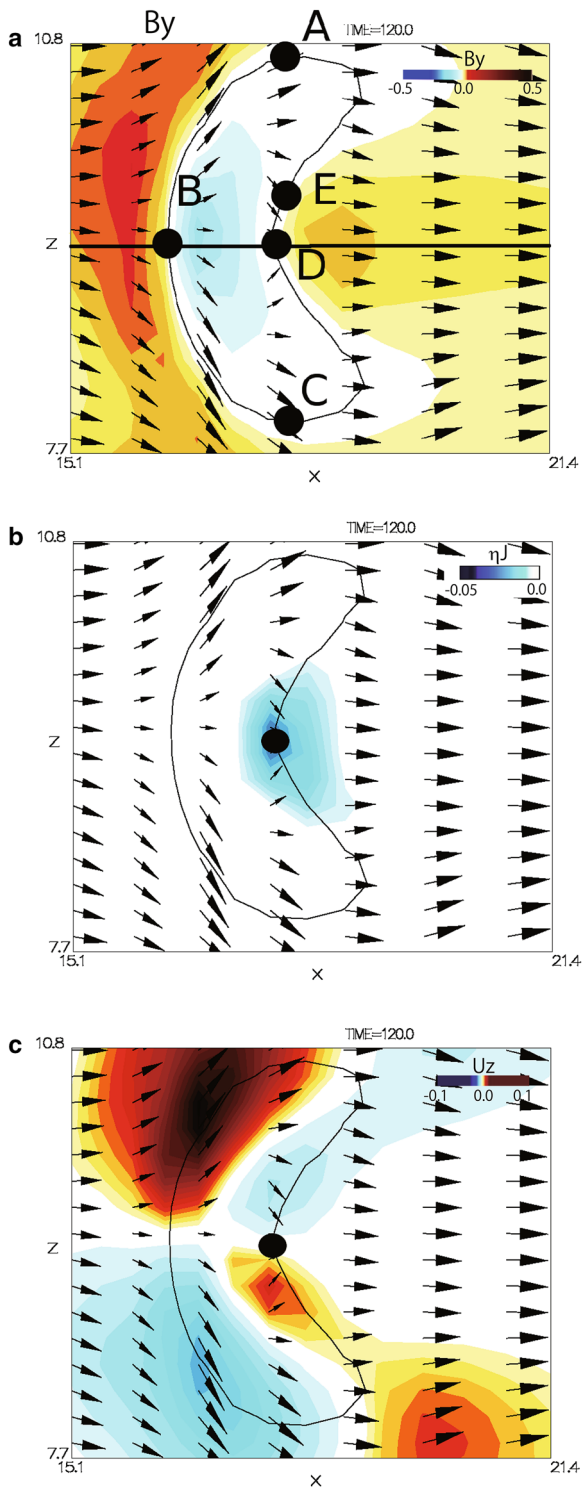

Fig. 5 Structure of the 3D plasmoid in event-5. Contour maps of (B_y, ηJ, U_z) are similar to those of a local area of Fig. 4. *Black arrows* are the plasma flow vector field (U_x, U_z). The *x*-directional *arrow's* maximum length on these figures has reached the Alfven speed measured in the upstream magnetic field region ($y > 1.0$). The scale of the *z*-directional *arrow's* length is emphasized by three times of the *x*-directional *arrow's* length. **a** B_y, **b** ηJ, **c** U_z

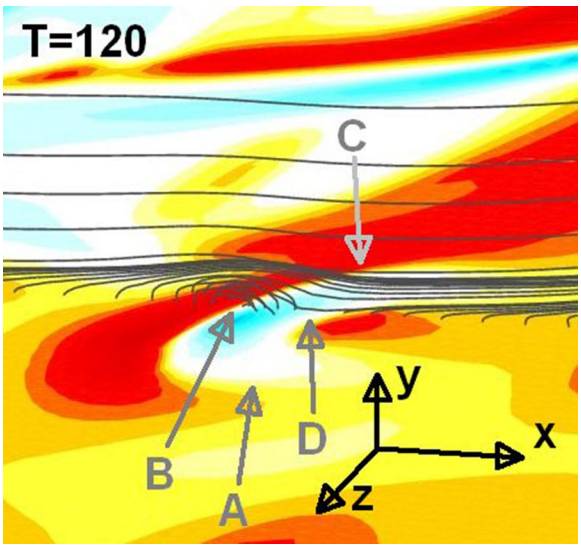

Fig. 6 Magnetic field lines and B_y contour map around 3D plasmoid in event-5

Figure 7 shows the time variation of the static pressure P, resistive electric field ηJ, and z-directional plasma flow velocity U_z plotted along the neutral line A–E–D–C in Fig. 5a. The abscissa is projected to z-axis. The uncolored (white) regions in Fig. 7a–c mean where x-line was not detected. For example, the colored contour region at $T = 105$, which is drawn on the bottom line of these three figures, is limited in $9.0 < z < 9.4$. It means that the x-line at $T = 105$ has the extent between $z = 9.0$ and $z = 9.4$. At $z = 9.0$ and $z = 9.4$, the x-line generally changes to the o-line, as shown at points A and C in Fig. 5a. As shown in these three figures, as time proceeds beyond $T = 105$, the x-line extends in z-direction. At $T = 129$ which corresponds to the most upper side of these figures, the x-line becomes wider beyond the extent of $7.5 < z < 10.5$ which is the z-directional full range of these figures.

In Fig. 7a, "P-min" labeled at $z = 9.2$ and $T = 115$ means the location of the minimum (static) pressure in the full range of Fig. 7a, which is colored by the deepest blue. In Fig. 7b, "ηJ-min" labeled at $z = 9.5$ and $T = 111$ is the minimum resistive electric field in the full range of Fig. 7b, which is colored by the deepest blue and means the center point of the most active magnetic diffusion region in the extent of the x-line. In Fig. 7c, the red and yellow colored regions mean the positive z-directional ($U_z > 0$) plasma flow regions. The rightward black arrow at $z = 9.1$ and $T = 114$ means the place at which the positive maximum U_z is detected. Similarly, the blue and green colored regions mean the negative z-directional ($U_z < 0$) plasma flow regions. The leftward black arrow at

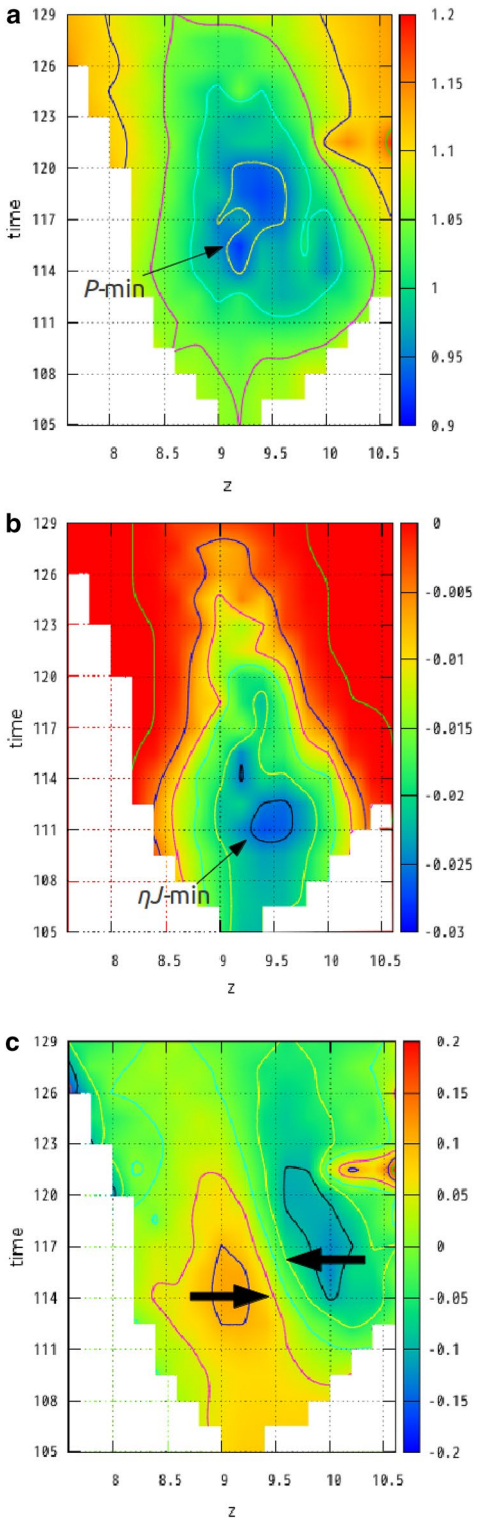

Fig. 7 Time variations of P, ηJ and U_z along the neutral line (x-line) in event-5. Abscissa is taken as the z-axis of simulation box where the z-axis is almost parallel to the neutral line. P-min and ηJ-min are, respectively, the peak points of the pressure decrease and resistive electric field. Also, two *black arrows* in (**c**) are the positive and negative peaks of the z-directional plasma flow U_z. **a** P, **b** ηJ, **c** U_z

$z = 10.0$ and $T = 116$ means the place at which the negative maximum U_z is detected. These maximum $|U_z|$ values reach about 15 % of the Alfven speed measured in the upstream magnetic field region, i.e., the lobe field region in magnetotail. Now, let us discuss what happens on the x-line of event-5, with Fig. 7a–c.

First, two black arrows in Fig. 7c mean the converging U_z reversal flows along the x-line, which seem to be driven by the pressure gradient along the x-line, because the converging U_z reversal flows are directed to the location of "P-min." In addition, since the plasma on the x-line is almost un-magnetized, there is no magnetic driving force to generate this U_z reversal. It may be noted that, as shown in the flow vector arrows of Fig. 5a, this converging U_z reversal is only observed around the x-line A–E–D–C and is not observed in the surrounding places. In fact, in Fig. 5a, the U_z reversal along o-line A–B–C is not converging. Rather, it is clearly diverging around point B and every other region separated from the x-line A–E–D–C and o-line A–B–C almost has no U_z component. Hence, the converging U_z reversal flows are generated by the pressure gradient along the x-line.

Second, since the timing of "P-min" appearance is a little delayed from that of "ηJ-min," the pressure gradient along the x-line may be considered to be generated by the fast reconnection process. As well known in numerical 2D studies (Ugai 1984, 1987a, b), when the impulsive fast reconnection process grows up, the pressure at x-point (x-line) rapidly decreases. Then, when the impulsive fast reconnection process is going to stop beyond the growth phase, i.e., in the recovery phase, the pressure at x-point slowly increases. Also, what happens in the 3D model on this paper is essentially the same as that of 2D model, but the z-directional fluctuations included in Eq. (3) may produce any z-directional inhomogeneity. When the pressure at the most active magnetic diffusion region (i.e., at point D in Fig. 5a) decreases faster than the pressure of the surrounding magnetic diffusion region (e.g., at points A, E and C in Fig. 5a), the fast reconnection process will produce the pressure gradient along the x-line, resulting in the converging U_z reversal flows along the x-line, as shown in Figs. 5c and 7c.

Third, in the view point of the MHD waves, the every x-directional variation caused in this 3D model is mainly driven by the Alfven wave which is the most essential driving mechanism of the reconnection process. On the other hand, the z-directional variation is mainly driven by the MHD fast wave, where the Alfven and MHD slow waves cannot almost propagate in the z-direction because there is no B_z component at $T = 0$ and, even after the reconnection process grew up, the B_z component still remains small all over the simulation box. Particularly, the MHD fast wave around x-line is degenerated to the sound

wave because of no magnetic field. Therefore, the z-directional development of the 3D fast reconnection process will be dominated by the local sound speed C_s, where C_s is initially set to be $0.98(=(\gamma P/2\rho)^{1/2}$, where $\gamma = 5/3$ is the specific heat ratio) in the center of the current sheet and almost does not vary through the simulation run. Considering simply in usual fluid dynamics, since the z-directional sound wave may cancel the z-directional inhomogeneity produced by the z-directional fluctuations in Eq. (3) and may prevent the 3D instability of the fast reconnection process. This will be true when the z-scale size of the inhomogeneity is sufficiently short. In other words, if the z-scale size of the 3D reconnection process is sufficiently small, the z-directional inhomogeneity will be effectively canceled and then the 3D instability does not occur or is weakened. Inversely, if the z-scale size is large, the pressure gradient generated by the fast reconnection process will survive and may be enhanced, leading to the enhancement of the 3D instability. In fact, this simulation run reveals that such enhancement of the pressure gradient driven by the fast reconnection process overcomes the cancelation driven by the sound wave. In other words, the x-directional Alfven wave overcomes the z-directional sound wave, leading to the 3D instability of the 2D fast reconnection process.

For event-5 shown in Figs. 5, 6 and 7, the z-scale size measured between those two thick black arrows in Fig. 7c is about $\Delta z = 0.9$, i.e., $(10.0 - 9.1)$. The sound waves take the traveling time $\Delta z/2C_s = 0.46$ to propagate from the center of the most active magnetic diffusion region to each point of "$|U_z|$-max," i.e., two thick black arrows in Fig. 7c. We may predict that this estimated time scale $\Delta z/2C_s$ determines the lifetime of event-5, if the z-directional sound wave effectively cancels the z-directional inhomogeneity and the pressure gradient along x-line. Nevertheless, the actual lifetime of event-5 measured in Fig. 7 is about $24 = 129 - 105$ (i.e., $105 < T < 129$) which is much longer than the predicted lifetime $\Delta z/2C_s$. It means that the fast reconnection process driven by the x-directional Alfven wave overcame the cancelation driven by the z-directional sound wave.

We conclude that the pressure gradient produced along x-line in the development of the 3D fast reconnection process drives the converging U_z reversal plasma inflow toward the most active magnetic diffusion region.

As discussed next, these features of the converging reversal inflow and pressure gradient seem to be consistent with some space satellite observations in which the density depletion (Nagai et al. 2013; Oieroset et al. 2000, 2001) is caused in the active reconnection site. Figure 8 schematically shows that the plasma along the x-line is flowing as U_z inflow toward the most active reconnection site.

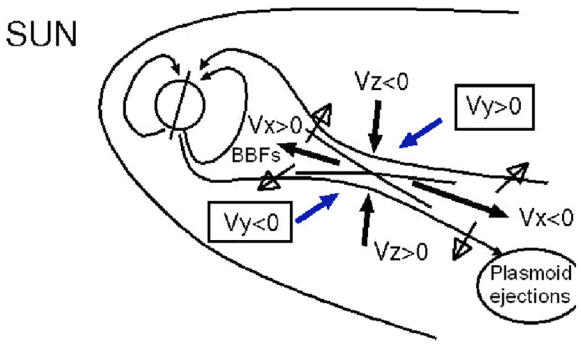

Fig. 8 Dawn–dusk (cross-tail) inflows in the current sheet of magnetotail are directed to the midnight from low-latitude boundary layer (LLBLs) of dawnside and duskside

Summary and discussions

In our previous papers (Shimizu et al. 2009a, b), it has been shown that the Petschek-type 2D fast magnetic reconnection process driven by the current-driven anomalous resistivity [Eqs. (4) and (5)] can be destabilized in 3D. This 3D instability is fully nonlinear because the z-directional size of the 3D fast reconnection region (e.g., shown in Fig. 5) is much smaller than the z-directional wave length $2L_z$ of the initial 3D resistive disturbance [Eq. (3)]. Evidently, the growth of the instability is not linear. It suggests that the 3D fast reconnection process strongly localized in the sheet current direction can be established even in a 1D current sheet without any distinct external disturbance strongly localized in the sheet current direction. A relation between the x-directional size and z-directional size of the 3D fast reconnection process was briefly studied in our previous paper (Shimizu et al. 2009a), but the relation between those sizes and $2L_z$ is still unclear and being now studied in detail.

Some recent bursty bulk flow (BBF) studies in the near-Earth magnetotail revealed that the cross-tail width of the BBF outflow is around 3-5Re which is much narrower than the width of the tail current sheet (Angelopoulos et al. 1996, 1997; Sergeev et al. 1999, 2000; Nakamura et al. 2004, 2005). It is still unclear why the BBFs are strongly localized in the sheet current (cross-tail) direction. Our study shown here suggests that BBFs generated by the 3D fast reconnection process can be strongly localized in the sheet current direction without any distinct externally driven mechanism to localize the reconnection region in the sheet current direction. In other words, once the 2D fast reconnection process is established in the 1D current sheet, it is consequently localized to the 3D fast reconnection process, due to the 3D instability. Our study does not answer how the 2D fast reconnection process can be triggered. However, any distinct externally driven mechanism is not needed to

localize the 3D reconnection process and keep them in a localized area of the much wider current sheet. Any weak plasma disturbances slightly perturbed in the sheet current direction are enough to localize the fast reconnection process in 3D.

With THEMIS observations of the near-Earth tail, Saito et al. (2011) reported that the thinning of the current sheet before the substrom onset is not necessarily accompanied by the intensification of the lobe field. The thinning of the current sheet and hence the substrom onset may be related to the fast reconnection process predicted in the magnetotail (Angelopoulos et al. 2008). If the 3D fast reconnection process is caused without such intensification of the lobe field, the 3D fast reconnection process may be caused by unknown internal process within the current sheet, which may be the 3D instability shown here.

As shown in Fig. 7, as the 3D fast reconnection process is developed, the pressure at an active reconnection site decreases and the pressure gradient along the x-line is formed. Then, it drives the plasma inflows along the x-line. According to our previous study (Figure 11 in Shimizu and Kondoh 2013), this pressure decrease is also observed in the x-directional pressure profile, i.e., along the plasma jet direction. Accordingly, such pressure decrease in the current sheet will be universally observable not only for cross-tail passing of satellite also for sun-earth direction passing.

In fact, with Geotail observations of magnetotail BBFs, Asano et al. (2004) and Nagai et al. (2013) reported the decrease in the plasma density in the active magnetic diffusion region. Also, Wind satellite (Oieroset et al. 2000, 2001) observed a similar density depletion in the magnetic diffusion region of electrons. Nagai et al. suggested that the pressure gradient generates the dawn–dusk plasma flows toward the active reconnection site at the duskside edge. Such a pressure gradient along the neutral line and plasma inflows are also observed in our study, as, respectively, shown in Fig. 7a, c.

It should be noted that the dawn–dusk (cross-tail) plasma flows along the x-line will be almost unmagnetized. Since such unmagnetized flow does not convey the magnetic field, it tends to prevent the thinning of the current sheet and may stop the 3D reconnection process, if there is no externally driven mechanism to keep the localized 3D reconnection process, such as the intensification of the lobe field. Our study shown here suggests that the 3D fast reconnection process in BBFs can grow in 3D, overcoming the unmagnetized plasma inflows due to the 3D instability.

At present, our studies cannot quantitatively explain why the BBFs are observed with about 3Re. The anomalous resistivity on the x-line may affect it as the resistive MHD effect, which will give the smallest limit size of this 3D instability. On the other hand, since the current sheet in the magnetotail should not be exactly 1D, the 2D or 3D structure of the magnetotail may give the largest limit size. These points must be studied in the near future.

Authors' contributions

TS and KK designed this study. TS and HT analyzed the data. TS drafted the manuscript. This work was done when HT was in Ehime university. All authors read and approved the final manuscript.

Acknowledgements

This work is supported by the Research Institute for Sustainable Humanosphere (RISH) of Kyoto University and Solar-Terrestrial Environment Laboratory (STEL) of Nagoya University. The numerical calculations were performed on the KDK computer system at RISH and parallel computer system at Nagoya and Kyoto University Data Processing Centers. The data analysis executed in this study was partially assisted by Mr. Imamura@ in Research Center for Space and Cosmic Evolution (RCSCE) of Ehime University. Authors thank them for these helps. Finally, authors thank for reviewers' helpful advices.

Competing interests

The authors declare that they have no competing interests.

Received: 26 September 2015 Accepted: 6 May 2016
Published online: 25 May 2016

References

Angelopoulos V, Coroniti FV, Kennel CF, Kivelson MG, Walker RJ, Russell CT, McPherron RL, Sanchez E, Meng CI, Baumjohann W, Reeves GD, Belian RD, Sato N, Friis-Christensen E, Sutcliffe PR, Yumoto K, Harris T (1996) Multipoint analysis of a bursty bulk flow event on April 11 1985. J Geophys Res 101(A3):4967–4989

Angelopoulos V, McFadden JP, Larson D, Carlson CW, Mende SB, Frey H, Phan T, Sibeck DG, Glassmeier KH, Auster U, Donovan E, Mann IR, Rae IJ, Russell CT, Runov A, Zhou X, Kepko L (2008) Tail reconnection triggering substorm onset. Science 321:931–935

Angelopoulos V, Phan TD, Larson DE, Mozer FS, Lin RP, Tsuruda K, Hayakawa H, Mukai T, Kokubun S, Yamamoto T, Williams DJ, McEntire RW, Lepping RP, Parks GK, Brittnacher M, Germany G, Spann J, Singer HJ, Yumoto K (1997) Magnetotail flow bursts: association to global magnetospheric circulation, relationship to ionospheric activity and direct evidence for localization. Geophys Res Lett 24(18):2271–2274

Asano Y, Mukai T, Hoshino M, Saito Y, Hayakawa H, Nagai T (2004) Current sheet structure around the near-Earth neutral line observed by Geotail. J Geophys Res 109:A02212

Forbes TG, Priest ER (1987) A comparison of analytical and numerical models for steadily driven magnetic reconnection. Rev Geophys 25(8):1583–1607

Nagai T, Shinohara I, Zenitani S, Nakamura R, Nakamura TKM, Fujimoto M, Saito Y, Mukai T (2013) Three-dimensional structure of magnetic reconnection in the magnetotail from Geotail observations. J Geophys Res 118:1667–1678

Nakamura R, Ammm O, Laakso H, Draper NC, Lester M, Grocott A, Klecker B, McCrea IW, Balogh A, Reme H, Andre M (2005) Localized fast flow disturbance observed in the plasma sheet and in the ionosphere. Ann Geophys 23:553–566

Nakamura R, Baumjohann W, Mouikis C, Kistler LM, Runov A, Volwerk M, Asano Y, Voros Z, Zhang TL, Klecker B, Reme H, Balogh A (2004) Spatial scale of high-speed flows in the plasma sheet observed by Cluster. Geophys Res Lett 31:L09804

Oieroset M, Phan TD, Lin RP, Sonnerup BUO (2000) Walen and variance analyses of high-speed flows observed by Wind in the midtail plasma sheet: evidence for reconnection. J Geophys Res 105:25247–25263

Oieroset M, Phan TD, Fujimoto M, Lin RP, Lepping RP (2001) In situ detection of collisionless reconnection in the Earth's magnetotail. Nature 412:414–417

Parker EN (1957) Sweet's mechanism for merging magnetic fields in conducting fluids. J Geophys Res 62:509–520

Petschek HE (1964) Magnetic annihilation. In: AAS-NASA symposium on the physics of solar flares, NASA Special Publ. (National Aeronautics and Space Administration, Washington, DC), SP-50, pp 425–439
Saito MH, Fairfield D, Le G, Hau LN, Angelopoulos V, McFadden JP, Auster U, Bonnell J, Larson D (2011) Structure, force balance, and evolution of imcompressible cross-tail current sheet thinning. J Geophys Res 116:A10217
Sergeev VA, Liou K, Meng CI, Newell PT, Brittnacher M, Parks G, Reeves GD (1999) Development of auroral streamers in association with localized impulsive injections to the inner magnetotail. Geophys Res Lett 26(3):417–420
Sergeev VA, Sauvaud JA, Popescu D, Kovrazhkin RA, Liou K, Newell PT, Brittnacher M, Parks G, Nakamura R, Mukai T, Reeves GD (2000) Multiple-spacecraft observation of a narrow transient plasma jet in the Earth's plasma sheet. Geophys Res Lett 27(6):851–854
Shimizu T, Kondoh K (2013) Magnetohydrodynami study of three-dimensional instability of the Petschek type magnetic reconnection. Phys Plasmas 20:122118
Shimizu T, Kondoh K, Shibata K, Ugai M (2009a) Magnetohydrodynamic study of three-dimensional instability of the spontaneous fast magnetic reconnection. Phys Plasmas 16:052903
Shimizu T, Kondoh K, Ugai M (2009b) Three-dimensional non-linear instability of spontaneous fast magnetic reconnection. Earth Planets Space 61:569–572
Shimizu T, Kondoh K, Ugai M, Shibata K (2009c) Magnetohydrodynamic study of three-dimensional fast magnetic reconnection for the intermittent snake-like downflows in solar flares. Astrophys J 707:420–427
Shimizu T, Ugai M (2000) Adiabatic expansion acceleration mechanism of superfast jets in the spontaneous fast magnetic reconnection model. Phys Plasmas 7:2417–2424
Shimizu T, Ugai M (2003) Magnetohydrodynamic study of adiabatic supersonic and subsonic expansion accelerations in spontaneous fast magnetic reconnection. Phys Plasmas 4:921–929
Ugai M (1984) Selfconsistent development of fast magnetic reconnection with anomalous plasma resistivity. Plasma Phys Control Fusion 26(12B):1549
Ugai M (1987a) Strong loop heating by the fast reconnection in a closed system. Geophys Res Lett 14:103–106
Ugai M (1987b) Nonlinear growth of fast reconnection in the long tearing-type field geometry. Phys Fluids 30(7):2163–2166
Ugai M (2010) Three-dimensional evolution of the fast reconnection mechanism in a sheared current sheet. Phys Plasmas 17:032313
Ugai M, Kondoh K, Shimizu T (2004) Computer studies on the three-dimensional spontaneous fast reconnection model as a non-linear instability. Phys Plasmas 11:1416–1423
Ugai M, Kondoh K, Shimizu T (2005) Spontaneous fast reconnection model in three dimensions. Phys Plasmas 12:042903
Ugai M, Tsuda T (1977) Magnetic field-line reconnection by localized enhancement of resistivity. J Plasma Phys 17:337–356
Vasyliunas VM (1975) Theoretical geophysics and space physics. Rev Geophys 13:303–336